Sensors and Materials, Vol. 38, No. 2 (2026) 529–532
MYU Tokyo

S & M 4316

Radioluminescence from Sm:CaI_2 for Scintillator Applications

Daisuke Nakauchi,* Takumi Kato, Noriaki Kawaguchi, and Takayuki Yanagida

Nara Institute of Science and Technology (NAIST), 8916-5 Takayama-cho, Ikoma, Nara 630-0192, Japan

(Received October 31, 2025; accepted December 16, 2025)

Keywords: NIR, photoluminescence, phosphor, single crystal, decay time

Sm-doped CaI_2 bulk crystals were synthesized by the vertical Bridgman method, and their photoluminescence and radioluminescence properties were systematically investigated. The samples exhibited a broad emission band centered around 870 nm, attributed to the 5d–4f transitions of Sm^{2+}. Decay curve analysis revealed the presence of two distinct components: a fast decay component (~0.6 μs) associated with self-trapped excitons, and a slow component (2–4 μs) corresponding to Sm^{2+} emission. These results suggest the potential applicability of Sm-doped CaI_2 crystals for photon-counting measurements in the NIR region.

1. Introduction

A scintillator is a luminescent material that emits light when exposed to ionizing radiation and has been widely employed in medical imaging, security, environmental monitoring, and resource exploration. Previous scintillator development has traditionally focused on phosphors emitting in the UV-visible range to match the sensitivity of photomultiplier tubes (PMTs),[1,2] whereas recent efforts increasingly emphasize red to NIR scintillators owing to potential advantages in emerging applications.[3–9] 600–900 nm is well matched to Si-based photodetectors such as Si photodiodes and avalanche photodiodes (APDs), enabling high scintillation output; in addition, light at these wavelengths is less absorbed by biological tissues, making red–NIR scintillators promising for *in vivo* monitoring and radiation therapy.

Sm^{2+} ions have attracted attention as novel emission centers that provide broad red–NIR emission arising from 5d–4f transitions, typically between 600 and 900 nm.[10–12] The emission spectrum of Sm^{2+} aligns with the spectral response of Si-based avalanche photodiodes, enabling efficient detection.[13–21] Furthermore, the ionic radius of Sm^{2+} is close to that of alkaline-earth ions, facilitating its incorporation into divalent cation sites. CaI_2 has a relatively high effective atomic number among halide hosts, and both undoped and Eu-doped CaI_2 have demonstrated high scintillation light yields of approximately 80000–100000 ph/MeV.[22] Although CaI_2 is strongly hygroscopic, the properties suggest that it is a promising host for Sm-based red–NIR scintillators. In this study, we investigated the luminescence and scintillation characteristics of Sm-doped CaI_2 single crystals to evaluate their potential as red–NIR scintillation materials.

*Corresponding author: e-mail: nakauchi@ms.naist.jp
https://doi.org/10.18494/SAM6032

ISSN 0914-4935
https://myukk.org/

2. Data, Materials, and Methods

0.3, 1, and 3 atomic% Sm-doped CaI_2 bulk crystals were synthesized by the Bridgman method. CaI_2 (99.9%), $SmCl_3 \cdot 6H_2O$ (99.9%), and 0.1 wt% graphite powders were put into a quartz ampoule and heated at 300 °C for 3 h. After sealing under vacuum as described previously,[23] crystal growth was performed using a Bridgman furnace (VFK-1800, Crystal Systems) with a growth speed of 5 mm/h. Photoluminescence (PL) quantum yields (QYs) and 3D emission spectra were measured using a Quantaurus-QY spectrometer (C11347, Hamamatsu Photonics). X-ray-induced radioluminescence (RL) spectra were measured using a spectrometer (QEPro, Ocean Insight), and RL decay profiles were evaluated using our original setup.[24] To measure pulse height (PH) spectra under ^{137}Cs γ-rays, a PMT (R7600-20, Hamamatsu Photonics) and nuclear instrument modules (556, 113, and 570, Ortec) were used with the shaping times of 10 μs for the samples and 0.5 μs for the reference Ce-doped Gd_2SiO_5 (GSO, 8000 ph/MeV, OXIDE).

3. Results and Discussion

Figure 1 shows the appearance of prepared Sm-doped CaI_2 polished with sandpaper for characterization. The polished samples were approximately 1 mm thick and exhibited a translucent appearance with a slight green tint. Figure 1 also shows the 3D PL spectra of Sm:CaI_2. A broad emission band is observed at 870 nm, which is suitable for Si-based photodetectors. Notably, the QY reached 61% at 1% Sm:CaI_2, while lower and higher concentrations (0.3% and 3%) yielded 31% and 17%, respectively. Compared with previously reported Sm-doped alkaline-earth halides—$CaCl_2$:Sm (750 nm), $SrCl_2$:Sm (690 nm), and $BaCl_2$:Sm (650 nm)[12,25]—the emission wavelength of Sm:CaI_2 is significantly longer. The observed redshift in CaI_2 suggests a weaker crystal field environment, supporting the expectation that iodide hosts can extend emission into the NIR region. Unlike previously reported Sm-doped phosphors, no emission due to the 4f–4f transitions of Sm^{3+} was observed, suggesting that Sm is predominantly incorporated as Sm^{2+} in CaI_2.

Figure 2 shows the X-ray-induced RL spectra of Sm:CaI_2 crystals. All the samples exhibit emission signals attributed to the 5d–4f transition of Sm^{2+} like in PL. 0.3% and 1% Sm:CaI_2 show a broad emission band at 410 nm, derived from self-trapped excitons (STEs), as reported previously.[25] The emission band was not detected in the PL under the tested excitation wavelengths because the reported excitation range for STE emission was 200–250 nm. The STE emission band decreases with Sm concentration owing to the absorption of Sm^{2+} at 430 nm shown in Fig. 1.

RL decay curves were measured and fitted using exponential functions, as shown in Fig. 3. The 3% Sm-doped sample exhibited a single decay component, which is attributed to the dominant Sm^{2+} 5d–4f transition observed in the RL spectrum. Although no available decay data for Sm^{2+} in CaI_2 have been reported, decay time corresponding to Sm^{2+} is expected to follow the empirical relationship $\tau \propto \lambda^3$. The measured decay time is consistent with the predicted trend reported in the literature.[26] Furthermore, Sm:CaI_2 exhibits a slightly longer decay time constant

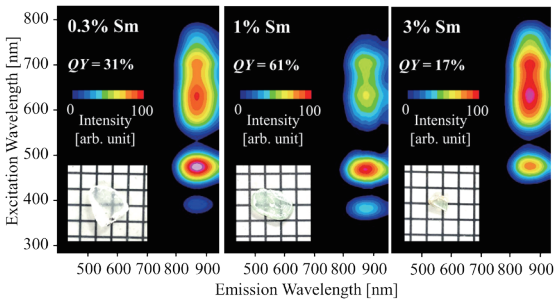

Fig. 1. (Color online) PL 3D spectra of Sm:CaI_2.

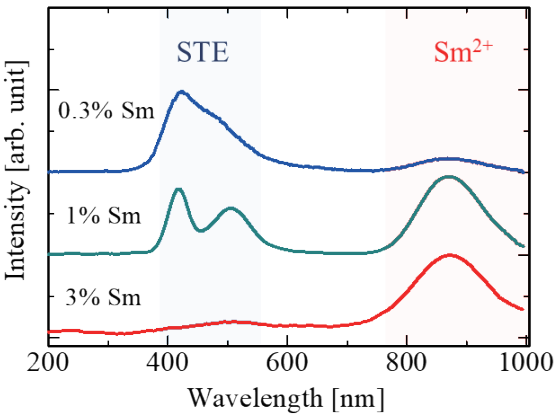

Fig. 2. (Color online) RL spectra of Sm:CaI_2.

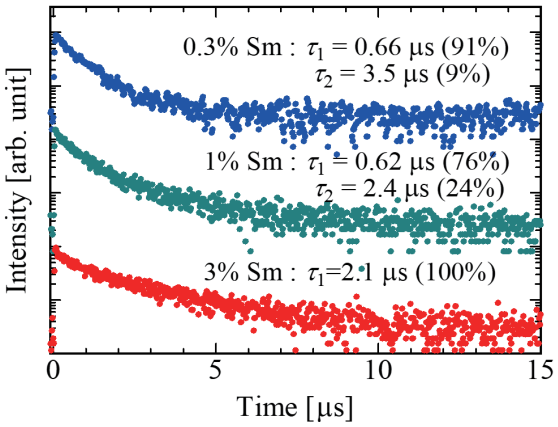

Fig. 3. (Color online) RL decay curves of Sm:CaI_2.

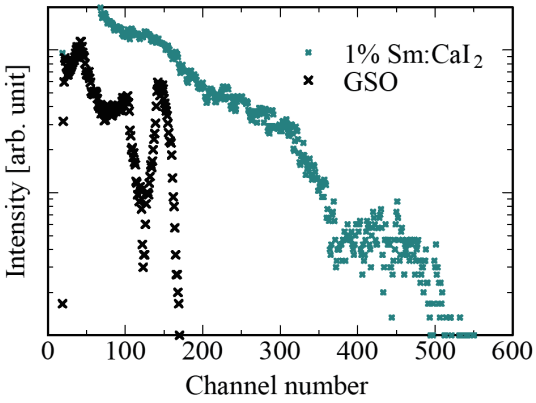

Fig. 4. (Color online) PH spectra of ^{137}Cs γ-rays.

(870 nm, 2.1 μs) than Sm:SrI_2 (750 nm, ~1.5 μs[15,17]), consistent with the longer emission wavelength. The 0.3% and 1% Sm-doped samples showed two decay components. On the basis of the spectral features and the relative intensity of the decay components, the slower component (τ_2~2–4 μs) is attributed to Sm^{2+} emission, whereas the faster component (τ_1~0.6 μs) is likely associated with STEs.

Figure 4 shows the PH spectra under γ-rays (662 keV) measured using 1% Sm:CaI_2 and GSO. Since the PMT used has negligible sensitivity at 870 nm, the LY of 1% Sm:CaI_2 is estimated to be ~24000 ph/MeV on the basis of the quantum efficiency at 410 nm. Although the RL spectrum is qualitative and does not allow direct intensity comparison, the emission at 870 nm is dominant over that at 410 nm in 1% Sm:CaI_2, suggesting a comparable LY in the NIR region.

4. Conclusions

Sm:CaI_2 bulk crystals were synthesized by the conventional vertical Bridgman method, and their PL and RL properties were systematically investigated. The samples exhibited a broad emission band centered at 870 nm, attributed to the 5d–4f transitions of Sm^{2+}. Decay curve

analysis revealed two distinct components: a fast component (~0.6 μs) due to STEs, and a slow component (2–4 μs) corresponding to Sm^{2+} emission. The LY is roughly estimated to be 20,000–30,000 ph/MeV, which is comparable to those of other Sm-doped materials such as Sm:$SrCl_2$ (34000 ph/MeV[20]), Sm:$SrBr_2$ (33000 ph/MeV[23]), and Sm:$CsBa_2I_5$ (20500 ph/MeV[27]). These results demonstrate that Sm:CaI_2 is capable of both NIR luminescence and γ-ray detection, indicating its potential for photon-counting applications in the NIR region. The emission band partially overlaps with the spectral sensitivity range of Si-APDs, suggesting that detection using Si-based photodetectors is feasible. Further optimization and integration with Si-APDs will be explored in future work.

Acknowledgments

This work was supported by JSPS KAKENHI (22H00309, 23K25126, 24K03197, and 25K08266), the Cooperative Research Project of Research Center for Biomedical Engineering, Research Foundation for the Electrotechnology of Chubu, and Shimadzu Science Foundation.

References

1 P. Dorenbos: Nucl. Instrum. Methods Phys. Res. B **486** (2002) 208.
2 M. Ishida, A. Watanabe, H. Kawamoto, Y. Fujimoto, and K. Asai: Sens. Mater. **37** (2025) 607.
3 P. Dorenbos: Opt. Mater. X **1** (2019) 100021.
4 Y. Endo, K. Ichiba, D. Nakauchi, T. Kato, N. Kawaguchi, and T. Yanagida: Sens. Mater. **36** (2024) 473.
5 M. Koshimizu, K. Tanahashi, Y. Fujimoto, and K. Asai: Sens. Mater. **37** (2025) 539.
6 H. Fukushima, R. Tsubouchi, T. Matsuura, T. Yoneda, and T. Yanagida: Sens. Mater. **37** (2025) 487.
7 S. Muneta, N. Kawano, D. Nakauchi, T. Kato, K. Okazaki, K. Ichiba, T. Kunikata, A. Nishikawa, K. Miyazaki, F. Kagaya, K. Shinozaki, and T. Yanagida: Sens. Mater. **37** (2025) 509.
8 S. Otake, S. Takase, T. Kato, D. Nakauchi, N. Kawaguchi, and T. Yanagida: Sens. Mater. **37** (2025) 519.
9 D. Nakauchi, T. Kato, N. Kawaguchi, and T. Yanagida: Sens. Mater. **37** (2025) 547.
10 Z. He, Y. Wang, S. Li, and X. Xu: J. Lumin. **97** (2002) 102.
11 L. C. Dixie, A. Edgar, and M. F. Reid: J. Lumin. **132** (2012) 2775.
12 M. Karbowiak, P. Solarz, R. Lisiecki, and W. Ryba-Romanowski: J. Lumin. **195** (2018) 159.
13 L. C. Dixie, A. Edgar, and M. C. Bartle: J. Lumin. **149** (2014) 91.
14 L. C. Dixie, A. Edgar, and C. M. Bartle: Nucl. Instrum. Methods Phys. Res. B **753** (2014) 131.
15 R. H. P. Awater, M. S. Alekhin, D. A. Biner, K. W. Krämer, and P. Dorenbos: J. Lumin. **212** (2019) 1.
16 W. Wolszczak, K. W. Krämer, and P. Dorenbos: Phys. Status Solidi - Rapid Res. Lett. **13** (2019) 1.
17 M. S. Alekhin, R. H. P. Awater, D. A. Biner, K. W. Krämer, J. T. M. De Haas, and P. Dorenbos: J. Lumin. **167** (2015) 347.
18 C. van Aarle, K. W. Krämer, and P. Dorenbos: J. Lumin. **251** (2022) 119209.
19 C. van Aarle, N. Roturier, D. A. Biner, K. W. Krämer, and P. Dorenbos: Opt. Mater. **145** (2023) 114375.
20 D. Nakauchi, Y. Fujimoto, T. Kato, N. Kawaguchi, and T. Yanagida: Crystals **12** (2022) 517.
21 D. Nakauchi, T. Kato, N. Kawaguchi, and T. Yanagida: Opt. Mater. **154** (2024) 115746.
22 R. Hofstadter, E. W. O'Dell, and C. T. Schmidt: Rev. Sci. Instrum. **35** (1964) 246.
23 D. Nakauchi, Y. Fujimoto, T. Kato, N. Kawaguchi, and T. Yanagida: Jpn. J. Appl. Phys. **60** (2021) 092002.
24 T. Yanagida, Y. Fujimoto, T. Ito, K. Uchiyama, and K. Mori: Appl. Phys. Express **7** (2014) 062401.
25 L. Dixie, A. Edgar, and M. Bartle: Phys. Status Solidi Curr. Top. Solid State Phys. **8** (2011) 132.
26 C. van Aarle, K. W. Krämer, and P. Dorenbos: J. Lumin. **266** (2024) 120329.
27 P. Dorenbos, K. W. Krämer, and M. S. Alekhin: Scintillator material comprising a crystalline metal halide codoped by Sm^{2+} and one other rare earth metal, WO/2019/137961, 2019.